Light-dressed States of H_2O in Intense Laser Fields

Shilin Liu, Akiyoshi Hishikawa, Atsushi Iwamae, and Kaoru Yamanouchi*

Department of Chemistry, School of Science, University of Tokyo, 7-3-1 Hongo, Bunkyo-ku, Tokyo 113-0033, Japan

The Coulomb explosion processes of H_2O, i.e., (i) $H_2O^{3+} \rightarrow H^+ + O^+ + H^+$ and (ii) $H_2O^{4+} \rightarrow H^+ + O^{2+} + H^+$, in ultrashort intense laser fields (~ 1 PW/cm^2) are investigated by the mass-resolved momentum imaging (MRMI) technique. From the analysis of these MRMI maps of the atomic fragment ions, it is found that the ∠H-O-H bond angle of the parent ions exhibits a significantly broad distribution (FWHM ~ 60^o) centered at the linear configuration and the O-H bond lengths for H_2O^{3+} and H_2O^{4+} become 1.7 and 2.0 times as long as R_e = 0.958 Å, respectively. The characteristic ultrafast bond angle deformation occurring prior to the Coulomb explosion is interpreted by the formation of the light-dressed potential energy surfaces of H_2O^+.

I. INTRODUCTION

With the development of short-pulsed laser technology in recent years, the magnitude of the electric field generated by the laser light can be raised as high as the Coulombic fields in molecules. Once a molecule is exposed to such a strong laser field, interaction between molecules and the laser field leads to a variety of new phenomena such as above-threshold dissociation (ATD), bond-softening and bond-hardening [1,2], spatial alignment of molecules [3] and formation of multiply charged ions followed by a Coulomb explosion process [4].

In the case of polyatomic molecules, as the laser field intensity increases, the *light-dressed potential energy surfaces* (LDPESs) begin to be formed through the coupling between molecular electronic states and the laser field. On the LDPESs, the molecular structural deformation occurs within an ultrashort laser pulse. If the subsequent ultrafast electron stripping process leads to the Coulomb explosion, the fragmentation pattern is expected to carry information on the geometrical structure of molecules deformed largely through the formation of LDPESs. The structural change of polyatomic molecules in intense laser fields was previously discussed by Cornaggia and co-workers for $C_2H_2^+$ [5], $C_3H_3^+$ [6],

CO_2 [7] and SO_2 [8] based on the coincidence patterns in a covariance map.

Since the momentum imposed on fragment ions depends sensitively on the geometrical structure of the parent ions just before the Coulomb explosion, information about the deformation of molecular skeletal structure can be derived directly by measuring the momentum vector of fragment ions produced in the Coulomb explosion process. Recently, we developed a method to visualize the momentum vector distribution of the fragment ions called *mass-resolved momentum imaging* (MRMI) [9-14], which has been successfully applied to diatomic [9-11] and triatomic [9, 12-14] molecules in intense laser fields of ~1 PW/cm^2, and has begun to be regarded as an efficient method by other groups [15,16]. As shown in our previous papers [13,14] and described briefly in section III.B, the geometrical structures of molecules just before the Coulomb explosion in intense laser fields can be determined directly by the analysis of the MRMI maps, and enable us to discuss the formation of LDPESs within an ultrashort intense laser pulse.

In our recent studies of CO_2 [13] and NO_2 [14], the analyses of the MRMI maps for the fragment ions showed that the structural deformation occurs not only along the bond-stretching coordinate but along the bending coordinate. Within the ultrashort laser-pulse duration (~100 fs), the $\angle$O-C-O angle distribution of CO_2 spreads significantly compared with the electronic ground state of neutral CO_2, while NO_2 evolves from its initial bent distribution towards a linear distribution. These structural deformations along the bending coordinate were attributed to the formation of LDPESs.

In the present work, we apply the MRMI method to the Coulomb explosion dynamics of H_2O in intense laser fields. In the laser-field intensity regime we achieved (~ 1.2 PW/cm^2), only two types of three-body Coulomb explosion channels were identified, i.e., $H_2O^{3+} \rightarrow H^+ + O^+ + H^+$ and $H_2O^{4+} \rightarrow H^+ + O^{2+} + H^+$, which are called the (1, 1, 1) and (1, 2, 1) pathways, respectively. Therefore, due to this limited number of fragmentation pathways, the geometrical structures of H_2O^{3+} and H_2O^{4+} just before the explosion can be determined with high-precision from the MRMI maps of the atomic fragment ions, and it becomes possible to discuss an effect of the formation of LDPESs in intense laser fields. Recently, the structural deformation of H_2O in intense laser fields was investigated by Sanderson *et al.* [15] using the MRMI method. In the present study, we aimed to derive more precise information about the distribution of the geometrical structure of the parent ions by properly taking into account the effect of the finite detector size.

II. EXPERIMENTAL

The details of our experimental setup were described previously [9-14]. The femtosecond laser system consists of a Ti:sapphire mode-locked oscillator and a regenerative amplifier, which produces amplified laser pulses (100 fs, $\lambda \sim 800$ nm) with a total energy of ~1 mJ/pulse at the repetition rate of 10 Hz.

The laser beam was focused by a quartz lens into a skimmed pulsed molecular beam with the H_2O gas in the region between the extraction parallel plates of a linear time-of-flight (TOF) mass spectrometer, where the extraction electric field of 234.2 V/cm was applied. In order to achieve a high angular resolution, a plate with a 10-mmϕ aperture was placed in front of the MCP ion detector. In our TOF mass spectrum with typical mass-resolution of $m/\Delta m \sim 620$, ion species with the different mass and charge numbers were separated well with no temporal overlap. The TOF mass spectrum with a high S/N ratio was obtained by accumulating the spectra for ~ 1000 laser shots using a digital oscilloscope at a 1 GHz sampling rate. When the nozzle was not operated, the background pressure in the main chamber was 1×10^{-8} Torr. Even during the nozzle operation, the pressure in the main chamber was kept below 6×10^{-8} Torr in order to avoid the space charge effect.

The angular distribution of the mass-resolved fragment ions was measured by rotating the polarization vector of the laser light with respect to the TOF axis. A total of 36 TOF mass spectra covering the 180^{o} polarization angle were measured to construct the MRMI maps.

III. RESULTS AND DISCUSSION

A. Overview of MS-TOF and MRMI maps

1. Two-body fragmentation pathway

In Fig. 1, the TOF mass spectrum of H_2O is shown, which was measured with the laser polarization direction parallel to the TOF axis. In the mass spectrum the fragment ions, H^+, O^{2+}, O^+ and OH^+, as well as the singly charged parent ions, H_2O^+, are identified.

The momentum vector distributions of the OH^+ and H^+ ions are shown in Figs. 2 (a) and (b), respectively, in a form of MRMI maps. The most probable two-body dissociation pathways to produce OH^+ are

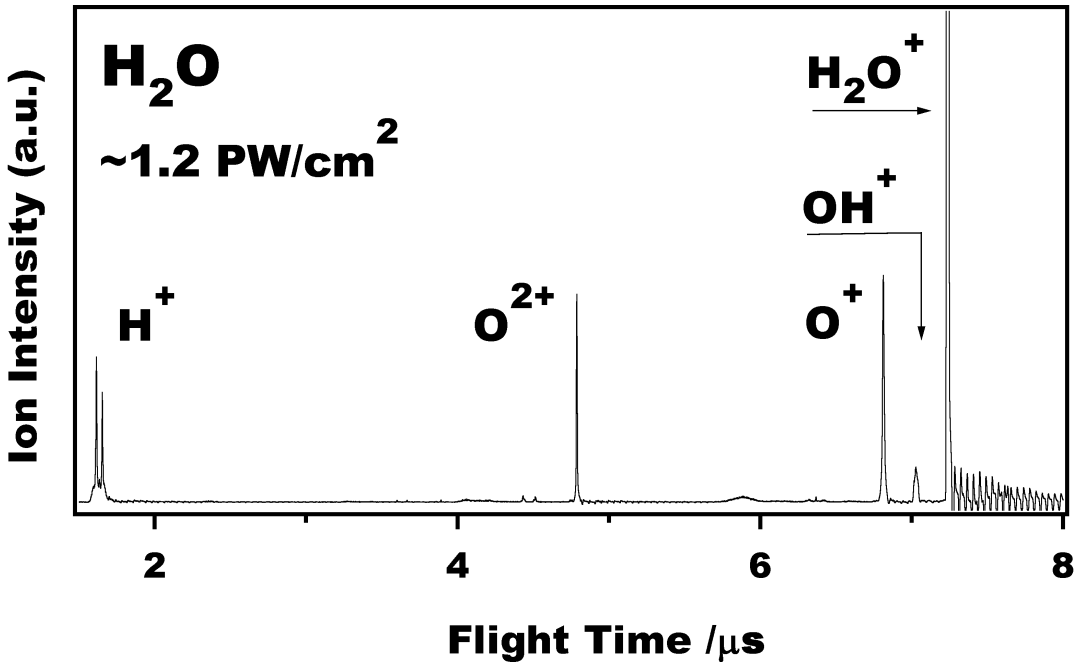

FIG. 1. The TOF mass spectrum of H_2O at λ = 800 nm with the laser field intensity of ~1.2 PW/cm^2 and the laser polarization direction parallel to the TOF axis.

$$\text{[0, 1] pathway:} \qquad H_2O^+ \rightarrow H + OH^+ \tag{1}$$

and

$$\text{[1, 1] pathway:} \qquad H_2O^{2+} \rightarrow H^+ + OH^+, \tag{2}$$

where a two-body pathway to form H^{p+} and OH^{q+} is denoted as a [p, q] pathway as in our previous study of N_2O [12]. It can be seen from Fig. 2(a) that (i) the momentum distribution of OH^+ is isotropic and (ii) there are at least two contributions, i.e., the central part within the momentum circle with a radius of ~20 $\times 10^3$ amu m/s and the peripheral part with the momentum radius of ~40 $\times 10^3$ amu m/s. On the other hand, the circular momentum distribution with a radius of ~40 $\times 10^3$ amu m/s can be seen in the MRMI map of H^+ in Fig. 2(b). Since the circular part in H^+ and the peripheral part in OH^+ have an overlap with each other, they are regarded as the [1, 1] pathway. The circular MRMI pattern for the [1, 1] pathway suggests that H_2O^{2+} is long-lived and its lifetime is comparable with or longer than a period of the molecular rotation. The central isotropic part in the OH^+ channel can be assigned mostly to the [0, 1] pathway.

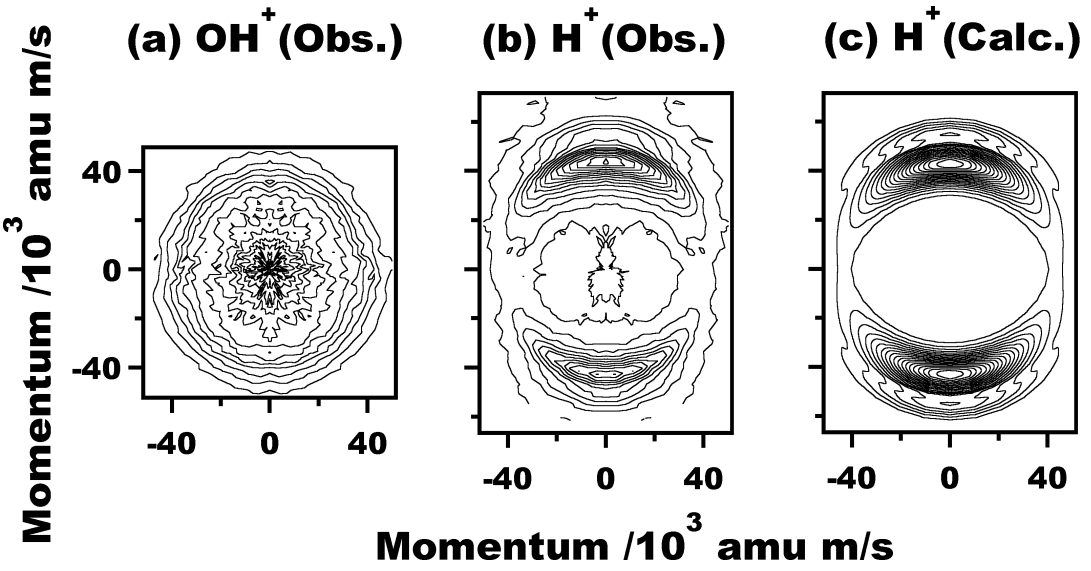

FIG. 2. The MRMI maps of (a) OH^+ and (b) H^+ observed at λ ~800 nm with the laser-field intensity of ~1.2 PW/cm^2 and (c) the best-fit MRMI map of H^+.

In Fig. 2(b), the weak central part can be assigned to the [1, 0] pathway,

$$\text{[1, 0] pathway:} \qquad H_2O^+ \rightarrow H^+ + OH, \tag{3}$$

which could compete with the [0, 1] pathway. Considering (i) the weak signal intensity of OH^+ in Fig. 1 compared with H^+, O^+ and O^{2+}, and (ii) the weak signal intensities of the [1, 0] and [1, 1] pathways in Fig. 2(b), the main dissociation pathways for H_2O ions in intense laser fields are the three-body fragmentation Coulomb explosion pathways.

2. Three-body fragmentation pathways

The MRMI map of H^+ in Fig. 2(b) exhibits a clear crescent-like pattern along the laser polarization direction. In the crescent pattern two components are identified, i.e., the inner and the outer crescent whose momentum centers are located at ~ 42×10^3 and ~ 56×10^3 amu m/s, respectively, which are assigned to the two three-body Coulomb explosion pathways; i.e.,

$$\text{(1, 1, 1) pathway:} \qquad H_2O^{3+} \rightarrow H^+ + O^+ + H^+ \tag{4}$$

and

$$\text{(1, 2, 1) pathway:} \qquad H_2O^{4+} \rightarrow H^+ + O^{2+} + H^+. \tag{5}$$

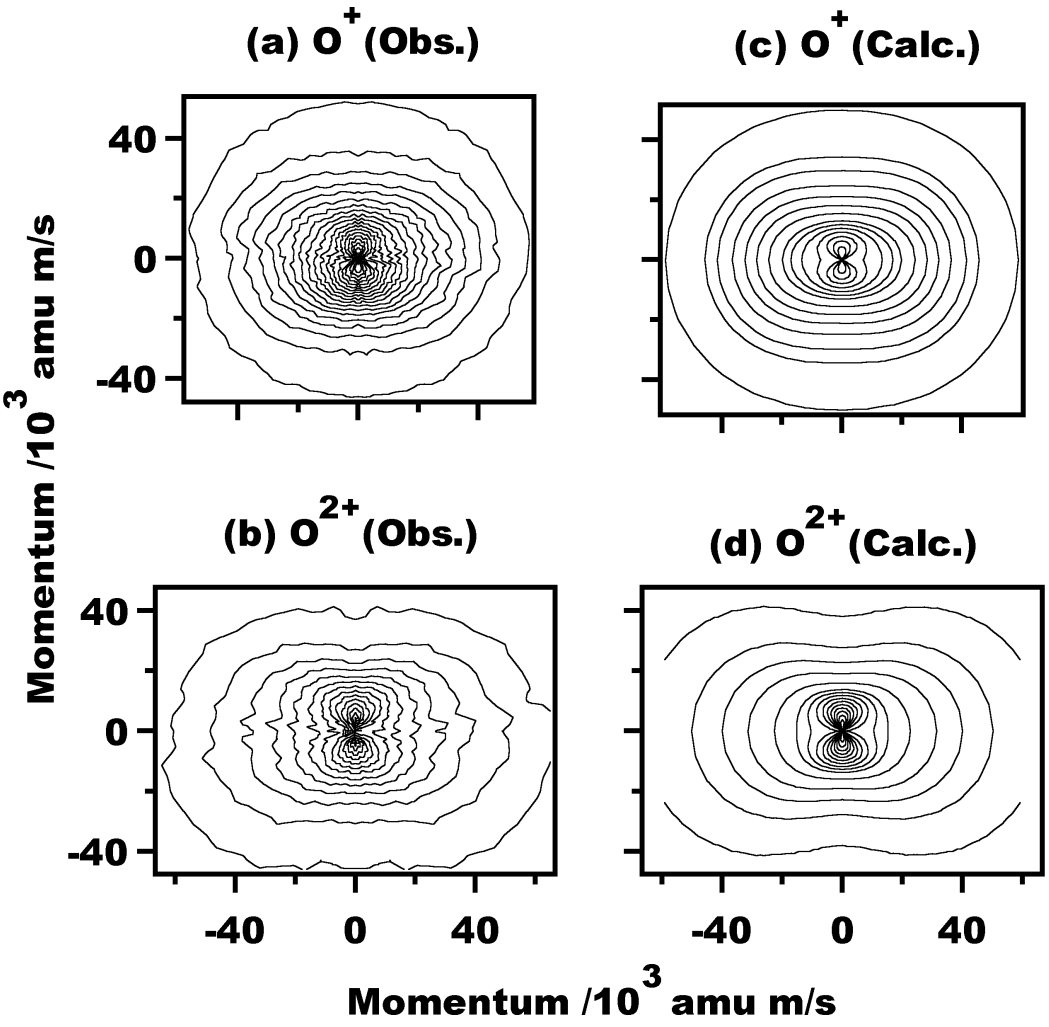

FIG. 3. The observed MRMI maps of (a) O^+ and (b) O^{2+} fragment ions and the best-fit MRMI maps of (c) O^+ and (d) O^{2+}.

The anisotropic momentum distribution pattern shows clearly that H^+ ions are ejected preferentially in the direction along the laser polarization vector, indicating that H_2O ions which undergo these three-body Coulomb explosions are prepared preferentially with the a-axis connecting the two hydrogen atoms parallel with the laser polarization direction.

In contrast to the three-body MRMI map of H^+, the MRMI maps of O^+ and O^{2+} in Fig. 3 exhibit elliptical patterns extending slightly towards the direction perpendicular to the laser polarization direction with the maximum intensity at zero momentum. Since the central oxygen ions stay at zero momentum only when H_2O ions take linear configuration, the observed elliptical distributions of O^+ and O^{2+} as well as the crescent distribution of H^+ spanning the

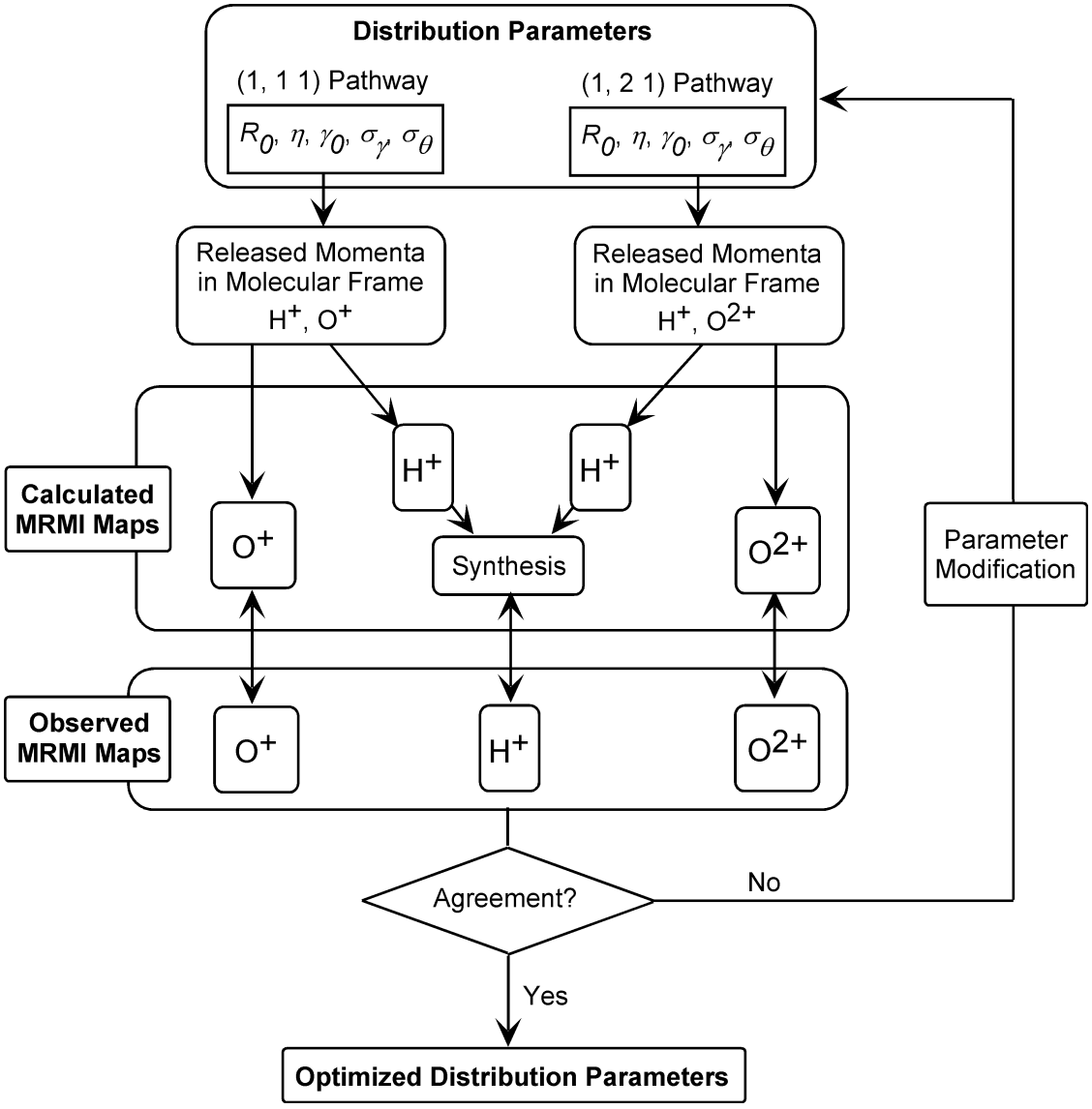

FIG. 4. Schematic diagram of the simulation procedure of the MRMI maps of H^+, O^+ and O^{2+} produced after the three-body Coulomb explosion of H_2O.

large angle indicate that the parent H_2O^{3+} and H_2O^{4+} ions prepared in the intense laser fields have a spread ∠H-O-H (= γ) distribution whose center is located at the linear configuration, i.e., $\gamma = 180^o$.

B. MRMI analysis

In order to derive quantitatively the information concerning the geometrical structure of

H_2O^{3+} and H_2O^{4+} just before the Coulomb explosion, we performed a trial-and-error simulation of the MRMI maps of all the fragment ions generated from the (1,1,1) and (1,2,1) pathways by taking the following steps [13, 14]: (i) the released momenta of the fragment ions are calculated for a given molecular geometry expressed by the O-H bond length, R(O-H), and the bond angle γ, and they are converted into the MRMI maps of H^+, O^+ and O^{2+} for a single explosion pathway by assuming the distributions of R(O-H) and γ, (ii) the MRMI map of H^+ is synthesized by adding the relevant single-pathway MRMI maps with their weights estimated from the observed yields of O^+ and O^{2+}, (iii) the geometrical parameters R(O-H) and γ are determined by comparing the synthesized and observed MRMI maps for all the fragment ions, and (iv) the steps (i) - (iii) are repeated with a new set of the geometrical parameters until the synthesized MRMI maps agree with the observed ones. The procedure of the simulation is schematically summarized in Fig. 4.

The geometry of the H_2O ions just before the explosion is expressed by the bond length distribution $F_R(R)$ [13,14] and the bond angle distribution $F_\gamma(\gamma)$ [13, 14, 17] as,

$$F_R(R) = \exp[-\eta(1/\sqrt{R} - 1/\sqrt{R_0})^2] \tag{6}$$

and

$$F_\gamma(\gamma) = \left\{\exp[-(\gamma-\gamma_0)^2/2(\sigma_\gamma/\sqrt{4\ln 2})^2] + \exp[-(\gamma+\gamma_0-2\mathrm{p})^2/2(\sigma_\gamma/\sqrt{4\ln 2})^2]\right\}^2, \tag{7}$$

where R_0, η, γ_0 and σ_γ, are the variable parameters. The spatial angular distribution of H_2O ions is described as [3]

$$F_\theta(\theta) = \exp[-\sin^2\theta/2\sigma_\theta{}^2], \tag{8}$$

where θ is the angle between the molecular a-axis and the laser polarization vector. The distribution width σ_θ is treated as a parameter representing the angular distribution of parent ions formed both by the torque given to H_2O from the laser field [3] and by the ionization enhancement [18] for a molecule whose θ is closer to zero. For given $F_R(R)$ and $F_\gamma(\gamma)$, the momentum distributions, $G(p_m,\theta_m{}^0)$s, of the fragment ions represented by the released momentum p_m and the ejection angle $\theta_m{}^0$ of the fragment ion in the molecular fixed frame are calculated for a given explosion pathway by numerically solving the classical equation of motion under the assumption that the repulsive forces between fragment ions are all

TABLE I. Optimized parameters for the geometrical and spatial-angular distributions determined from the trial-and-error simulation of the MRMI maps of H^+, O^+ and O^{2+}.[a)]

	R_0 /Å	η	γ_0 /deg	σ_γ/deg	σ_θ /deg
(1, 1, 1) pathway	1.6(1)	100(20)	180	60(10)	20(3)
(1, 2, 1) pathway	1.9(1)	150(30)	180	60(10)	17(2)

[a)] Numbers in parentheses represent the estimated limits of error.

Coulombic.

From the one-dimensional momentum distribution, the two-dimensional MRMI map is constructed in terms of the Legendre polynomials, P_{2k}'s, as

$$I(p_{//}) = \int_{|p_{//}|}^{p_{\max}} \frac{G(p_m,\theta_m^0)}{2p_m}[\sum_{k=0}^{\infty} a_{2k} P_{2k}(\cos\theta_m^0) P_{2k}(\cos\alpha) P_{2k}(p_{//}/p_m)]dp_m \,, \quad (9)$$

where α denotes the angle between the laser polarization vector and the TOF axis. The coefficients a_{2k}'s are determined by the Legendre expansion of the spatial angular distribution function $F_\theta(\theta)$. The $p_{\max}$ defined as

$$p_{\max} = [p_{//}^{\,2} + (\frac{md}{2t_0})^2]^{1/2} \quad (10)$$

represents the upper limit of the released momentum of the fragment ions that can reach the detector with an effective diameter d and the flight time t_0 [10-14]. The MRMI maps for a single Coulomb explosion pathway are then synthesized for all the respective fragment ions.

The ratio of the relative yields for the (1,1,1) and (1,2,1) pathways, I(1,1,1) and I(1,2,1), was derived to be I(1,1,1) : I(1,2,1) = 1.0 : 0.25, by fitting the momentum-scaled (MS) TOF spectrum of H^+ with two Gaussian momentum distributions. The geometrical parameters, γ_0, σ_γ, R_0, η and σ_θ, were adjusted in a trial-and-error simulation of the observed MRMI maps of H^+, O^+ and O^{2+} in a manner described above so that all the MRMI maps are reproduced simultaneously. The simulation of the MRMI maps revealed that (i) the extent of the spread and that of the ellipticity of the MRMI maps of O^+ and O^{2+} are sensitive to γ_0 and σ_γ, respectively, (ii) the magnitudes of the central momentum and the width of the momentum

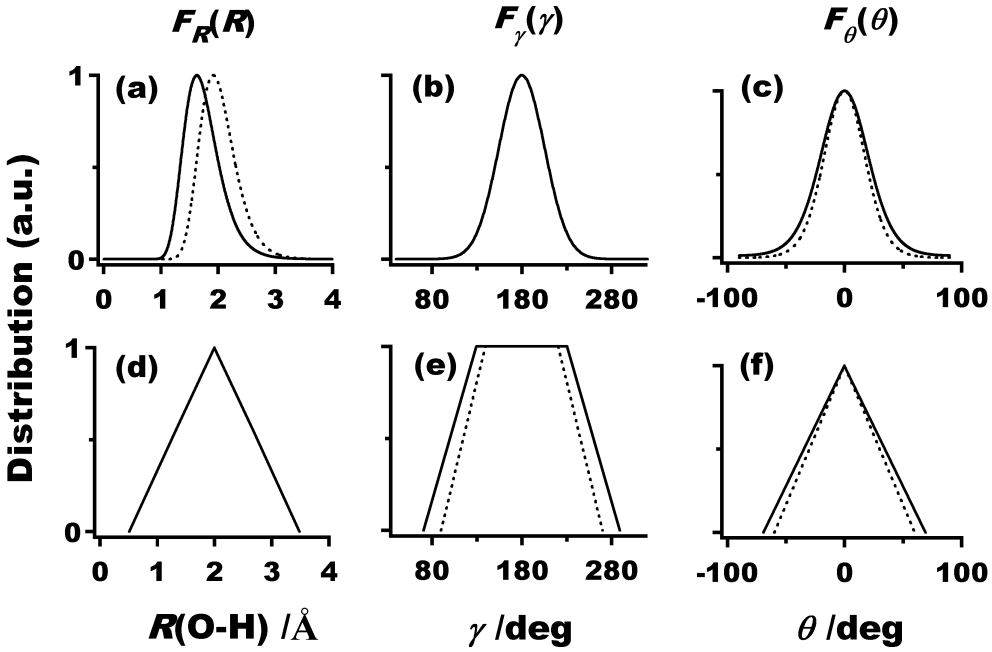

FIG. 5. Optimized distributions, $F_R(R)$, $F_\gamma(\gamma)$ and $F_\theta(\theta)$, of H_2O^{3+} (solid curve) and H_2O^{4+} (dashed curve) just before the Coulomb explosion derived in the present study, (a) - (c), and in Ref. 15, (d) - (f). The same γ distributions are obtained for H_2O^{3+} and H_2O^{4+} in (b).

distribution of H^+ are sensitive to R_0 and η, respectively, and (iii) the angular distribution of H^+ is sensitive to σ_θ. Therefore, these five parameters were determined with only small correlations.

The best-fit MRMI maps for H^+, O^+ and O^{2+} obtained after several trial-and-error iterations are shown in Fig. 2(c) for H^+ and in Fig. 3 for O^+ and O^{2+}, which reproduce well the corresponding observed MRMI maps. The optimized parameters are listed in Table I, and the distributions of $F_R(R)$, $F_\gamma(\gamma)$ and $F_\theta(\theta)$ are shown in Fig. 5. The corresponding distribution function obtained recently by Sanderson *et al.* [15] are also shown for comparison.

As seen in Fig. 5(a), the bond length for the parent ions tends to become larger with the charge number increases, i.e., R_0s for H_2O^{3+} and H_2O^{4+} are 1.7(1) and 2.0(1) times longer than that in the neutral electronic ground state (R_e(O-H) = 0.958Å), respectively. This type of bond elongation in intense laser fields was observed for diatomic molecules, I_2 [19], N_2 [10] and NO [11], and triatomic molecules, CO_2 [13] and NO_2 [14], indicating the existence of a common dynamical mechanism determining the bond elongation processes.

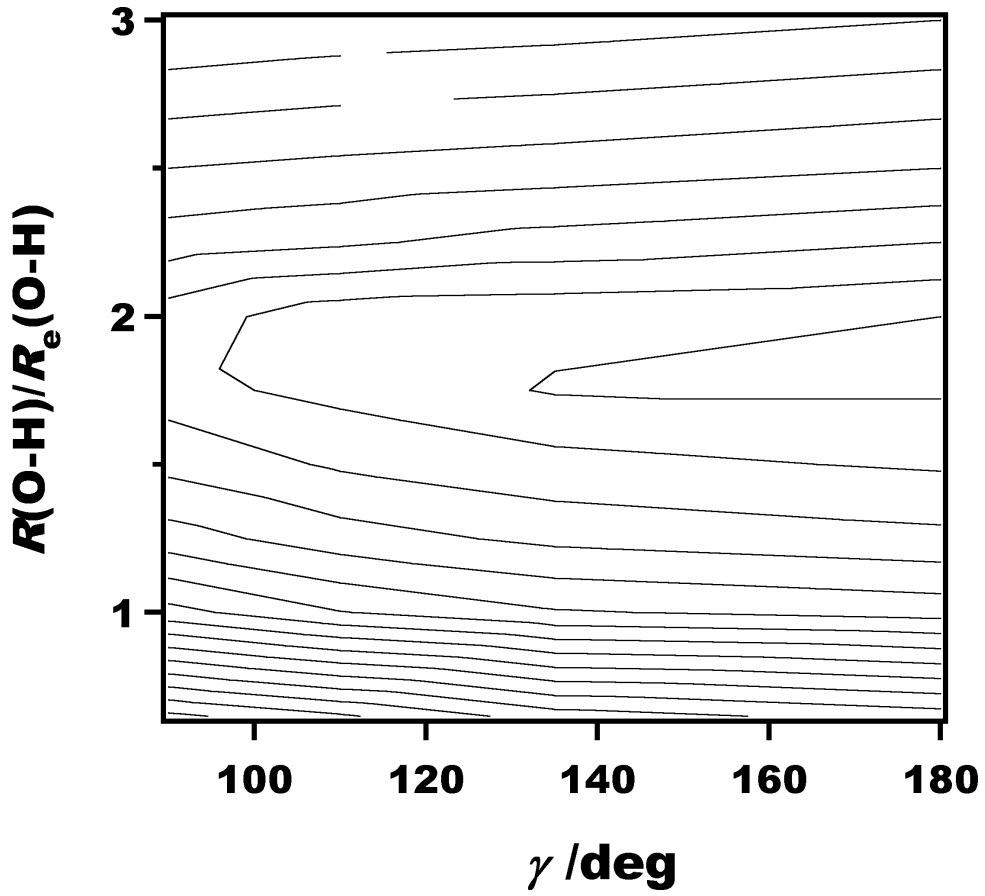

FIG. 6. The calculated appearance intensities of the laser field as a function of the bond length scaled by R_e(O-H) and the ∠H-O-H bond angle, γ, for the (1, 1, 1) Coulomb explosion pathway based on the classical field ionization model.

In contrast to the bent geometry of neutral H_2O in the electronic ground state ($\gamma = 104.5^o$), both of the bond angle distributions of H_2O^{3+} and H_2O^{4+} in Fig. 5(b) exhibit a large extent ($\sigma_\gamma = 60^o$) of spread whose center is located at 180^o. It can be said that H_2O changes its geometry in intense laser fields from the initially bent geometry to the linear geometry.

There are two types of interaction which make the spatial angular distribution narrower, i.e., (i) the laser-induced torque which aligns a molecule along the laser polarization direction, and (ii) the enhanced ionization when the molecular a-axis is close to the laser polarization direction. Therefore, the determined width, σ_θ, of the spatial angular distribution is regarded as an effective parameters. However, it should be noted that the geometrical structure and its distribution represented by R_0, η, γ_0 and σ_γ are extracted free from the spatial angular distribution as far as the anisotropic distributions of the ejected fragment ions are expressed as

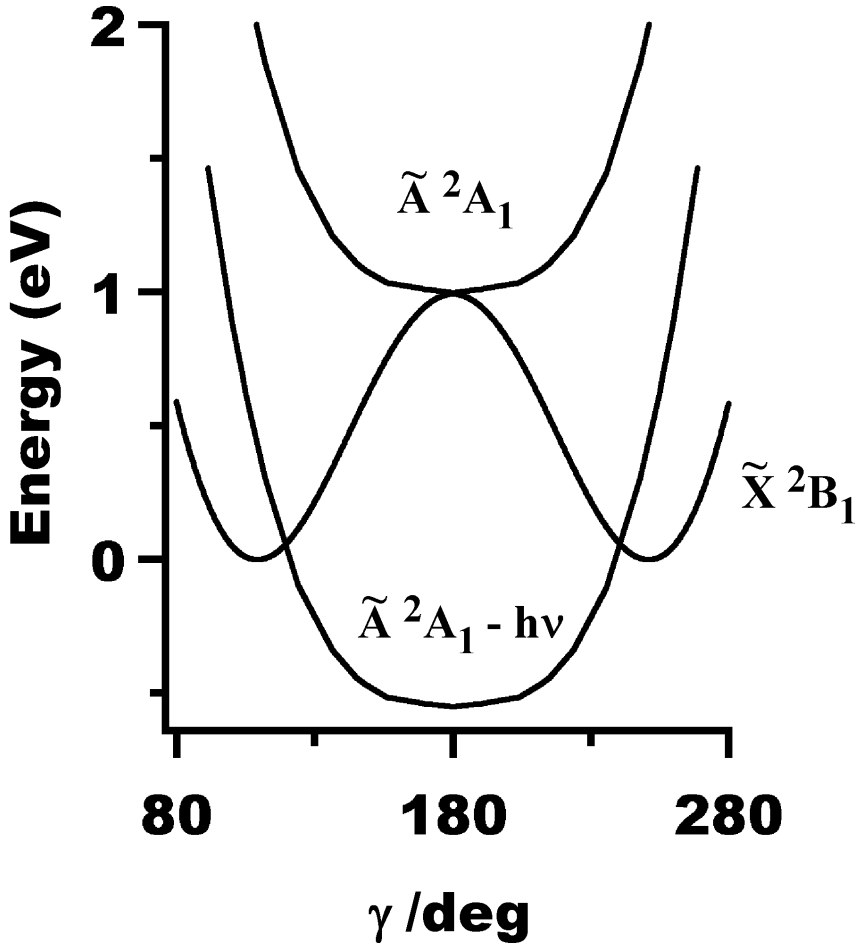

FIG. 7. Potential functions along the bending coordinate of the $\tilde{A}^2A_1$, $\tilde{X}^2B_1$ and light-dressed $\tilde{A}^2A_1$ states of H_2O^+, drawn using the theoretical potential functions (Ref. 26) of the $\tilde{A}^2A_1$ and $\tilde{X}^2B_1$ states derived when R(O-H) = 0.997 Å.

a sum of the Legendre products in Eq. (9).

C. Structural deformations of H_2O

1. Bond elongation

From the MRMI analysis the bond length distributions for H_2O^{3+} and H_2O^{4+} were determined to have peaks at R(O-H)/R_e(O-H) = 1.7(1) and 2.0(1), respectively. It has been reported experimentally [20, 21] as well as theoretically [22, 23] that the ionization rate of

small molecules in intense laser fields is significantly enhanced at elongated bond length and reaches a maximum at $R \sim 2R_e$. By applying the classical field-ionization model [21], the appearance laser intensity for the generation of H_2O^{3+} and H_2O^{4+} was calculated as a function of R(O-H) and γ when the a-axis of H_2O is fixed in the direction parallel to the laser polarization vector. The derived appearance intensities are plotted as a two-dimensional map in Fig. 6.

It was found that (i) the critical geometrical parameters, R_c(O-H) and γ_c, at which the appearance intensity takes a minimum is R_c(O-H)/R_e(O-H) = 1.8 and $\gamma_c = 180^o$, and (ii) the appearance intensity depends only weakly on the bending angle. Therefore, the γ_c value has a large uncertainty and is not defined well. The calculated dependence of the appearance intensity on the bond length explains well quantitatively the derived bond length distribution of H_2O^{3+} and H_2O^{4+} shown in Fig. 5(a). This behavior of the ionization appearance intensity, i.e., its weak dependence on the bond angle and sensitive dependence on the bond length, was also identified for CO_2 [13] and NO_2 [14], and is considered to be a common feature of triatomic molecules in intense laser fields.

2. Bond-angle deformation

In order to explain the derived broad bond-angle distribution shown in Fig. 5(b), the formation of LDPESs in intense laser fields was inferred, on which the ultrafast bond angle deformation occurs. As suggested by Rottke *et al.* [24] and Sanderson *et al.* [15], the phenomenon responsible for this spread of the bond angle centered at 180^o can be ascribed to the potential softening along the bending coordinate caused by the coupling between the bent ground $\tilde{X}^2B_1$ state ($\gamma_e = 120^o$) and the linear excited $\tilde{A}^2A_1$ state of H_2O^+ in intense laser fields. When λ = 800 nm, the one-photon dressed state of $\tilde{A}^2A_1$ crosses with the bent $\tilde{X}^2B_1$ state near the two equivalent equilibrium positions of the double-minimum well of the $\tilde{X}^2B_1$ state as shown in Fig. 7, which was drawn based on an *ab initio* MRCI calculation by Brommer *et al.* [25]. The γ distribution could spread due to the laser-induced population transfer to the excited state having a linear geometry through the one-photon crossing points at which a significant avoided crossing occurs to form a pair of adiabatic LDPESs. Then, the lower counterpart of the LDPESs could drive the ultrafast nuclear motion towards the linear structure within the ultrafast laser-pulse duration.

IV. SUMMARY

The ultrafast nuclear deformation processes of H_2O ions in intense laser fields were investigated by measuring the MRMI maps of the fragment ions produced by the two three-body Coulomb explosion processes, i.e., $H_2O^{3+} \rightarrow H^+ + O^+ + H^+$ and $H_2O^{4+} \rightarrow H^+ + O^{2+} + H^+$.

From the analysis of the MRMI maps, it was found that (i) the O-H bond lengths of H_2O^{3+} and H_2O^{4+} respectively become 1.7(1) and 2.0(1) times longer than that of the neutral H_2O in the electronic ground state, and (ii) the $\angle$H-O-H bond angle becomes ~180^o with a Gaussian distribution width of 60^o(10) for both of the two parent ions. The observed geometrical deformation was interpreted by the formation of LDPESs by the one-photon coupling between the bent ground $\tilde{X}^2B_1$ state (γ_e = 120^o) and the linear excited $\tilde{A}^2A_1$ state of H_2O^+ in intense laser fields.

ACKNOWLEDGMENT

The present work was supported by the CREST (Core Research for Evolutionary Science and Technology) fund from Japan Science and Technology Corporation.

* Author to whom correspondence should be addressed.

[1] A. D. Bandrauk, *Molecules in intense laser fields*, (M. Dekker Pub., New York, 1993).

[2] A. Giusti-Suzor, F. H. Mies, L. F. DiMauro, E. Charron, and B. Yang, *J. Phys. B* **28**, 309 (1995).

[3] B. Friedrich and D. Herschbach, *Phys. Rev. Lett.* **74**, 4623 (1995).

[4] K. Codling and L. J. Frasinski, *J. Phys. B* **26**, 783 (1993), and references therein.

[5] C. Cornaggia, M. Schimit and D. Normand, *Phys. Rev. A* **51**, 1431 (1995).

[6] C. Cornaggia, *Phys. Rev. A* **52**, R4328 (1995).

[7] C. Cornaggia, *Phys. Rev. A* **54**, R2555 (1996).

[8] C. Cornaggia, F. Salin and C. LeBlanc, *J. Phys. B* **29**, L749 (1996).

[9] A. Hishikawa, A. Iwamae, K. Hoshina, M. Kono and K. Yamanouchi, *Chem. Phys. Lett.* **282**, 283 (1998).

[10] A. Hishikawa, A. Iwamae, K. Hoshina, M. Kono and K. Yamanouchi, *Chem. Phys.* **231**, 315 (1998).

[11] A. Iwamae, A. Hishikawa and K. Yamanouchi, *J. Phys. B* **32**, 223 (2000).

[12] A. Hishikawa, A. Iwamae, K. Hoshina, M. Kono and K. Yamanouchi, *Res. Chem. Intermed.* **24**, 765 (1998).

[13] A. Hishikawa, A. Iwamae and K. Yamanouchi, *Phys. Rev. Lett.* **83**, 1127 (1999).

[14] A. Hishikawa, A. Iwamae and K. Yamanouchi, *J. Chem. Phys.* **111**, 8871 (1999).

[15] J. H. Sanderson, A. El-Zein, W. A. Bryan, W. R. Newll, A. J. Langley and P. F. Taday, *Phys. Rev. A* **59**, R2567 (1999).

[16] J. H. Posthums, J. Plumridge, P. F. Taday, J. H. Sanderson, A J. Langley, K. Codling and W. A. Bryan, *J. Phys. B***32**, L93 (1999).

[17] T. Graber, E. P. Kanter, Z. Vager and D. Zaifman, *J. Chem. Phys.* **98**, 7725 (1993).

[18] J. H. Posthumus, J. Plumridge, M. K. Thomas, K. Codling, L. J. Frasinski, A. J. Langley and P. F. Taday, *J. Phys. B***31**, L553 (1998).

[19] G. N. Gibson, M. Li, C. Guo and J. P. Nibarger, *Phys. Rev. A***58**, 4723 (1998).

[20] J. H. Posthums, A. J. Giles, M. R. Thomspon and K. Codling, *J. Phys. B* **29**, 5811 (1996).

[21] E. Constant, H. Stapefelt and P. B. Corkum, *Phys. Rev. Lett.* **76**, 4140 (1996).

[22] T. Seideman, M. Y. Ivanov and P. B. Corkum, *Phys. Rev. Lett.* **75**, 2819 (1995).

[23] S. Chelkowski, T. Zuo, O. Atabek and A. D. Bandrauk, *Phys. Rev. A* **52**, 2977 (1995).

[24] H. Rottke, C. Trump, and W. Sandner, *J. Phys. B* **31**, 1083 (1998).

[25] M. Brommer, B. Weis, B. Follmeg, P. Rosmus, S. Carter, N. C. Handy, H. Werner and R. J. Knowles, *J. Chem. Phys.* **98**, 5222 (1993).